Materials Physics and Mechanics. 2022;50(2): 331-341
Research article
http://dx.doi.org/10.18149/MPM.5022022_12

Submitted: July 15, 2022
Approved: September 8, 2022
Accepted: October 3, 2022

Kinetics of the microstructure of targets from FCC alloys under high-strain-rate deformation

S.A. Atroshenko[1,2]✉, M.S. Smakovsky[3], G.G. Savenkov[4]

[1]Institute for Problems of Mechanical Engineering RAS, 61, Bolshoi Pr. V.O., St. Petersburg, Russia, 199178

[2]St. Petersburg State University, Universitetskaya embankment, 7/9, St. Petersburg, Russia, 199034

[3]JSC "Armalit", st. Trefoleva, 2, St. Petersburg, Russia

[4]St. Petersburg Institute of Technology (Technical University), 26, Moskovskiy prospect, St. Petersburg, Russia, 190013

✉ satroshe@mail.ru

Abstract. The protection of various objects experiencing shock loads from the impact of irregularly shaped impactors with impact velocities over 1.5-2.0 km/s is of considerable interest and is relevant. Computer modeling of the processes of high-speed interaction of impactors with various objects in order to create optimal designs requires deep knowledge of the physical and mechanical properties and processes occurring in the thickness of at least the material of the barrier (object). However, the existing technical measuring instruments make it possible to register only the kinematic parameters of the deformation and destruction of the barrier and impactor, while the development of internal processes remains inaccessible for visualization. In addition, the physical processes of high-speed deformation and destruction occurring in obstacles are highly dependent on the many contact boundaries that are inherent in irregularly shaped strikers, and in computer modeling and experimental studies, strikers, as a rule, have the correct geometric shape (cylinder, sphere). As a result, there is a significant loss of calculation accuracy. The article is devoted to the analysis of the behavior of various FCC metals – aluminum alloys, stainless steel, and aluminum bronze under impact loading by irregularly shaped projectiles with velocities of 1.5-2.0 km/s. Transformations of the deformed state of materials are revealed and it is shown that they depend little on the initial structure.

Keywords: Aluminum alloy, stainless steel, aluminum bronze, shock loading

Acknowledgements*. Atroshenko S.A. received financial support for this study under grant N 22-11-00091 of Russian Science Foundation.*

Citation: Atroshenko SA, Smakovsky MS, Savenkov GG. Kinetics of the microstructure of targets from FCC alloys under high-strain-rate deformation. *Materials Physics and Mechanics*. 2022;50(2): 331-341. DOI: 10.18149/MPM.5022022_12.

1. Introduction

Protection of various modern technical objects experiencing high-energy loads from the impact of irregularly shaped strikers (for example, ammunition fragments, micrometeorites, etc.) with impact velocities over 1.5-2.0 km/s is of significant scientific and practical interest. In this case, the strain rates in the material reach ~ 10^5 s^{-1} and more. Computer simulation of

© S.A. Atroshenko, M.S. Smakovsky, G.G. Savenkov, 2022.
Publisher: Peter the Great St. Petersburg Polytechnic University
This is an open access article under the CC BY-NC 4.0 license (https://creativecommons.org/li-censes/by-nc/4.0/)

the processes of high-speed interaction of strikers with various objects in order to create optimal structures requires deep knowledge of the physical and mechanical properties and processes occurring in the thickness, at least of the material of the target (object). However, the existing technical measuring instruments make it possible to register only the kinematic parameters of deformation and destruction of the obstacle and the striker, while the development of internal processes remains inaccessible for visualization. In addition, the physical processes of high-speed deformation and fracture occurring in obstacles are highly dependent on the set of contact boundaries that are inherent in irregularly shaped strikers, and in computer modeling and experimental studies, strikers, as a rule, have the correct geometric shape (cylinder, sphere). As a result, there is a significant loss in the accuracy of calculations.

Therefore, the study of the evolution of the microstructure of the target material under the conditions of a high-speed impact with an irregularly shaped striker comes to the fore, despite the fact that such studies are of a post-factor nature and the state of the microstructure at the moment of dynamic action may differ from that after dynamic loading. But it can be noted that it is the processes of restructuring the internal structure of the material during its dynamic deformation and destruction that determine the physical and mechanical properties of the medium.

Dynamic processes have a multiscale character, as shown in [1], the scale levels of destruction in the spall zone of steel during longitudinal shear and normal separation differ by 1-1.5 orders. The authors of the work [2] show the presence of 4 scale levels in the D-16 aluminum alloy under shock loading. The destruction as a result of dynamic loading of the samples is explained by the dispersion of particle velocities (elementary strain carriers) at different scale-structural levels of deformation and destruction. High-speed fracture most often occurs at an intermediate between the macroscopic and microscopic structural level (mesoscopic), corresponding to the scale of the internal structure of the material [3], and this fact also complicates the interpretation of the results obtained. Dynamic processes occurring at the mesoscale level, as a rule, are nonequilibrium, unstable and chaotic [4-6].

An equally important task is to study changes in the evolution of the microstructure in a lower range of strain rates $\dot{\varepsilon}$ =10^2-10^3 s^{-1}. In particular, this concerns multiphase alloys with an FCC lattice.

2. Samples, materials, and experimental technique

In this work, we studied the microstructure of samples cut from targets made of an aluminum alloy of the AMg6 type (but additionally doped with scandium), BrAlFeNiMn_9-4-4-1 tin-free aluminum bronze, and 18Cr-10Ni-Ti stainless steel (sufficiently detailed information about these materials is given in [7], pierced by irregularly shaped compact impactors (otherwise called impact "cores" [8,9]). The initial velocity of the impact of the striker with the obstacle was ~ 1.8-2.0 km/s. In addition, samples from BrAlFeNiMn_9-4-4-1 were studied after testing by the Kolsky method on a split Hopkinson bar (SHB) [10] with different strain rates. The SHB technique allows one to determine various properties of materials precisely in the specified range of strain rates, which is included in a wider range of strain rates of 10^3-10^5 s^{-1} [11]. The maximum speeds of this range are realized using the direct impact method, the Taylor method, and the thin ring expansion method loaded with an electromagnetic pulse, or other short microsecond pulses [12,13,14]. Samples for metallographic studies were cut from targets with a diameter of 90 mm and a thickness of 11 mm. A view of an aluminum alloy target after penetration is shown in Fig. 1a. Samples prepared for metallographic studies are shown in Fig. 1b, 1c.

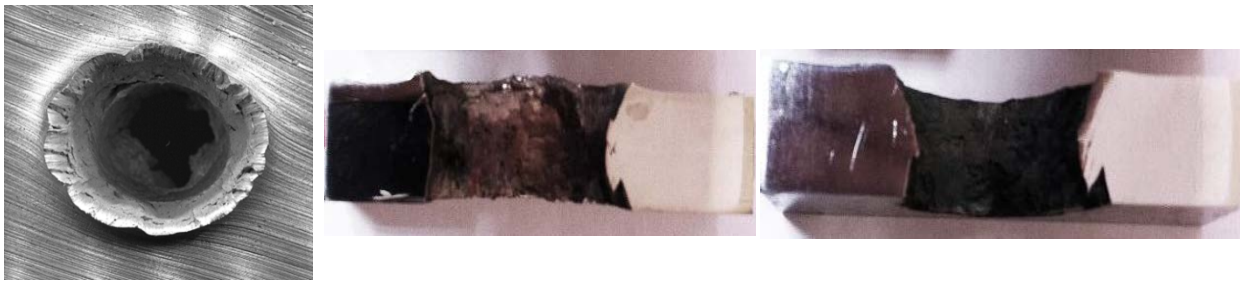

a) b) c)

Fig. 1. General view of an aluminum target after penetration (a) and samples for metallographic studies (b, c): b – stainless steel, c – aluminum bronze

A rod (similar to 90 mm in diameter) annealed at 800ºC for three hours, 18 mm in diameter and 450 mm in length was chosen as the initial semi-finished product of BrAlFeNiMn_9-4-4-1 tin-free aluminum bronze for research at the SHB.

The statical mechanical characteristics of the investigated alloys were as follows: $\sigma_{0,2} = 325$ MPa, $\sigma_B = 430$ MPa, $\delta_5 = 25\%$, $\psi = 30\%$ – for aluminum alloy; $\sigma_{0,2} = 275$ MPa, $\sigma_B = 620$ MPa, $\delta_5 = 59\%$, $\psi = 70\%$ – for stainless steel; $\sigma_{0,2} = 385$ MPa, $\sigma_B = 725$ MPa, $\delta_5 = 35\%$, $\psi = 36\%$ – for aluminum tin-free bronze.

Tests on the SHB were carried out at three strain rates $\dot{\varepsilon}$: $\dot{\varepsilon}$ = 915 s^{-1}, $\dot{\varepsilon}$ = 1475 s^{-1}, $\dot{\varepsilon}$ = 1750 s^{-1}. The mechanical properties of the samples obtained at these speeds are presented in Table 1.

Table 1. Dynamic properties of bronze BrAlFeNiMn_9-4-4-1

Strain rate, $\dot{\varepsilon}$, s^{-1}	Yield strength, σ_{Sd}, MPa	Tensile strength σ_{bd}, MPa	Relative elongation δ_d, %	Relative narrowing ψ_d, %
915	480 ± 5	665 ± 15	30 ± 1,0	39 ± 2,5
1475	505 ± 15	710 ± 20	29,5 ± 0,5	39 ± 1,0
1750	610 ± 10	695 ± 55	31 ± 1,0	40 ± 3,0

The structure was studied using an Axio-Observer Z1 M optical microscope in a bright field and in C-DIC contrast. The initial structures of the studied alloys are shown in Fig. 2.

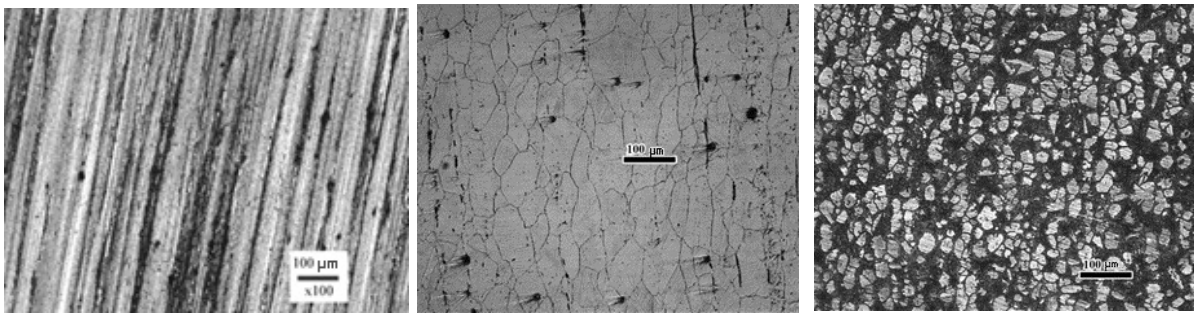

a) b) c)

Fig. 2. Initial structures of the investigated alloys: a – aluminum alloy; b – steel; c – bronze

3. Results of microstructural studies of samples after high-velocity impact and their analysis

General remarks and results. In our case, all targets are classified as obstacles of finite thickness. In this case, the mutual influence of the cavity formation zone and the rear free surface becomes a significant factor [15,16]. The compression wave caused by the impact is reflected from the free surface in the form of a tensile wave, which has time to return to the cavity even before the plastic flow of the material stops. If the duration and amplitude of tensile stresses exceed the critical values, then the destruction of the barrier material near the rear surface occurs – it is spalling. If a spall does not form, the unloading changes the stress-strain state in the cavity formation zone (compression along one axis is transformed into a volumetric oppositely deformed state), which contributes to the facilitated penetration of the obstacle by the striker. In our studies, for all three samples on the rear surface, zones of destruction were revealed, which are obviously associated with spalling phenomena (Fig. 1).

In all targets, irrespective of the alloy grade, nodal points between the so-called terrace ledges were found in the macro-relief of the surfaces of the holes formed [17].

Also, in the punched targets, 3 (stainless steel and aluminum bronze) or 4 (aluminum alloy) penetration zones are distinguished (Fig. 1). The first zone, due to the non-stationary stage of penetration [18], corresponds to the depth of ~ 0.3 - 0.5 of the penetration thickness and, the second (and the third for the barrier made of aluminum alloy) ~ 1/3 of the thickness (stationary stage of penetration), the third (the fourth, for the aluminum alloy) (associated with spalling phenomena) ~ 1/6 - 1/3 of the thickness.

Evolution of microstructure in aluminum alloy. The original stripe structure (Fig. 2a) at the very top of the ridge changes to a fragmented one (Figs. 3a - 3b), which indicates large plastic deformations and high temperatures in this layer. As the projectile velocity decreases, the strip structure remains unchanged (Fig. 3c), however, periodic protrusions are formed along the edge of the cavity (Fig. 3d).

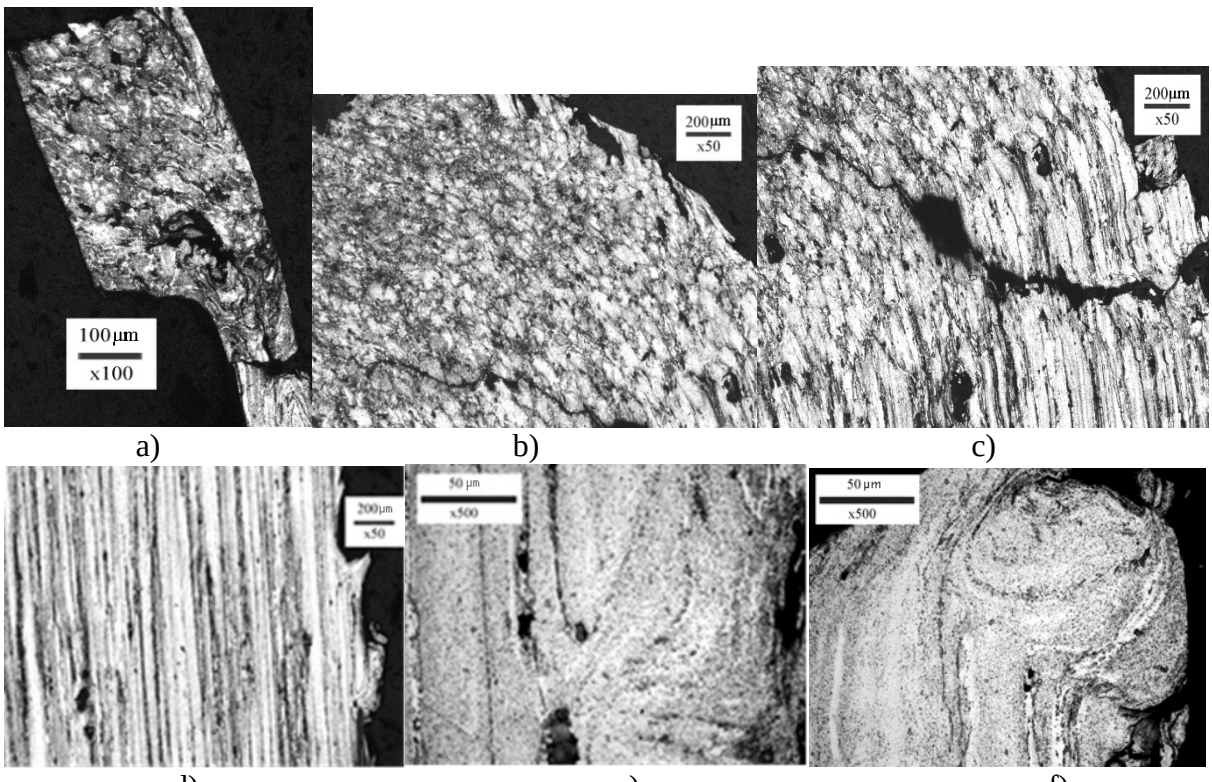

Fig. 3. Consecutive change of the profile of the relief as the target is penetrated

The formation of such protrusions may be due to the fact that as the striker moves, the temperature of the material in front of it increases; in combination with high pressures, this can lead to the appearance of local areas of melting and, accordingly, to a decrease in the friction force. This leads to stress release and a change in the friction mechanism from dry to plastic. The transition to a section with a lower temperature creates some stoppers for the movement of the striker, which again leads to a change in the friction mechanism from plastic to dry. Such a sequence of changes in mechanisms and the appearance of stoppers can lead to the appearance of periodic protrusions.

And, finally, when the speed of the striker becomes much less than the initial one, rotational (vortex) modes of plastic deformation begin to appear intensively (Fig. 3e, d). One of the probable causes of the vorticity of the target material may be that as the projectile velocity decreases, the material in front of it may already be in a friable state due to the appearance of tensile stresses arising from the interaction of the forward and backward unloading waves. Friability of the material increases the number of degrees of freedom, which can lead to the formation of structures that experience pure rotation due to shear stresses.

Microstructure evolution in stainless steel. As noted above, there are three zones of penetration in the stainless steel barrier (Fig. 1b), corresponding to three stages of penetration.

In the first zone, at a distance of 1.5-3.8 mm from the frontal surface and 0.15-0.75 mm from the edge of the cavity, an area of rotational plastic deformation was found, consisting of disks with a practically ideal circular shape. The radius of the discs ranges from 35 to 325 μm (Fig. 4). Inside the large circles are smaller circular elements and friable elements (pores). The microhardness inside the circular formations is higher than the initial hardness of the material outside these regions (HV = 2.62 GPa) by ~ 25% and on average is HV ≈ 3.14 GPa. Near the circular formations, closer to the edge of the cavity, adiabatic shear bands (ASB) were found, which are apparently associated with a high local temperature near the contact surface between the impactor and the target [19] and with the instability of plastic flow resulting from the effect of thermal softening at adiabatic or almost adiabatic plastic deformation. It can be assumed that at the first stage of penetration when the velocity parameters of the striker are still sufficiently high, the target material does not have time to dissipate the mechanical energy of the striker due to the collective motion and multiplication of dislocations. Therefore, to maintain the dissipation rate at the required level, additional rotational modes of plastic deformation are switched on [20].

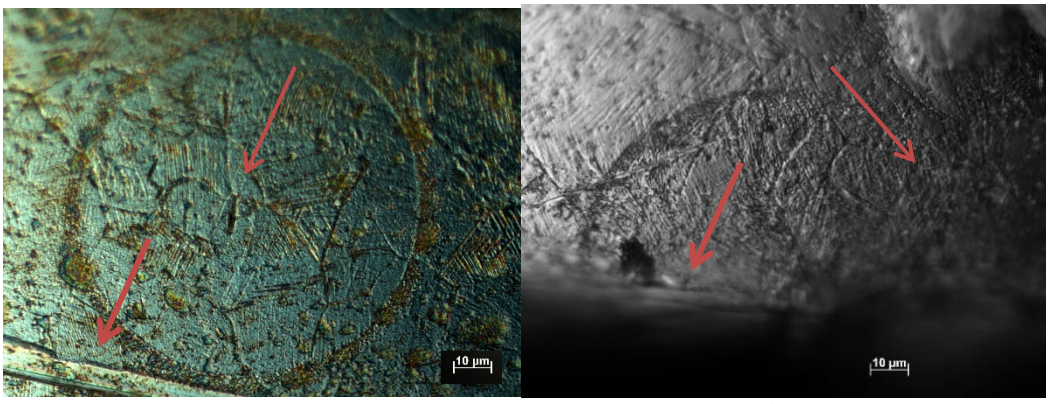

a) b)

Fig. 4. Region of rotational plasticity ×1000 (a, b) (thin arrows indicate small circular formations, thick arrows indicate adiabatic shear bands)

The second stage of penetration is characterized by the formation of a wavy relief of the cavern edges on the contact surface between the striker and the target material. Signs of rotational (wave-like) plastic deformation inside the grain structure (Fig. 5b) were found in

the same way as for the first zone. In addition, this zone is characterized by recrystallization processes, which manifest themselves in the form of crumbling of ferrite colonies (Fig. 5c) or coarsening of grains (Fig. 5d).

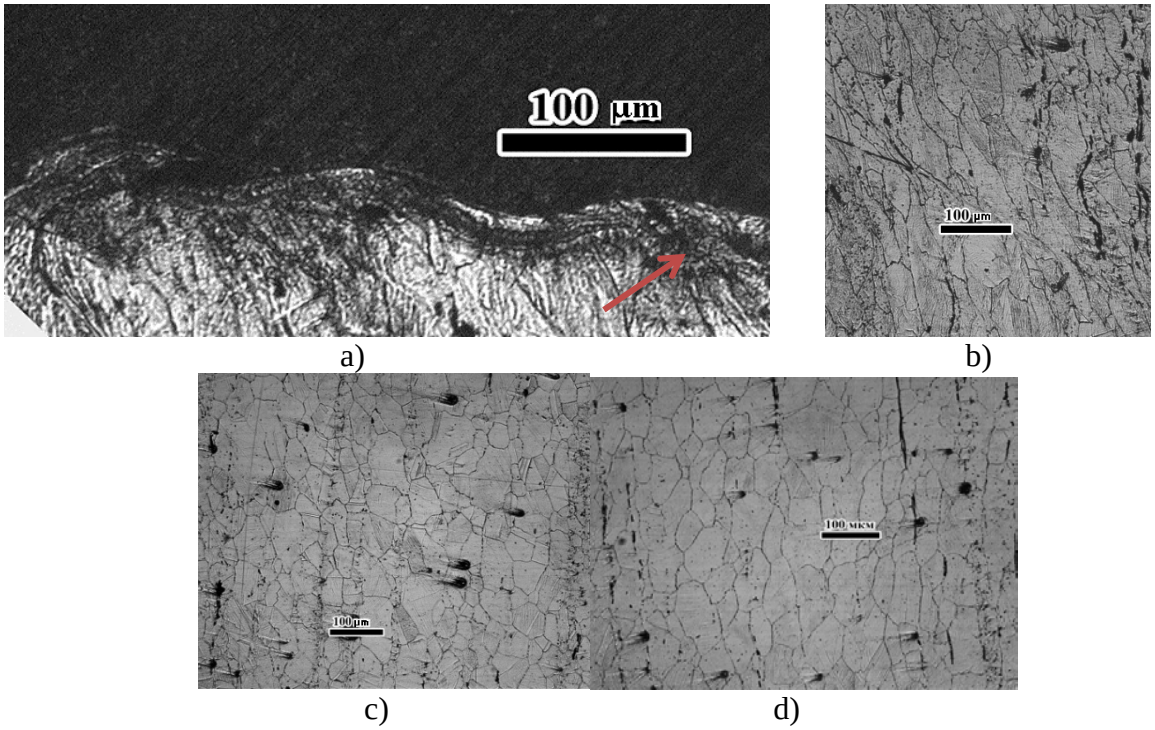

a) b)

c) d)

Fig. 5. Steel microstructure in the second target zone: ASB (indicated by an arrow) and wavy traces of plastic deformation – (a, b), crushing of δ-ferrite colonies – (c) and traces of grain coarsening – (d)

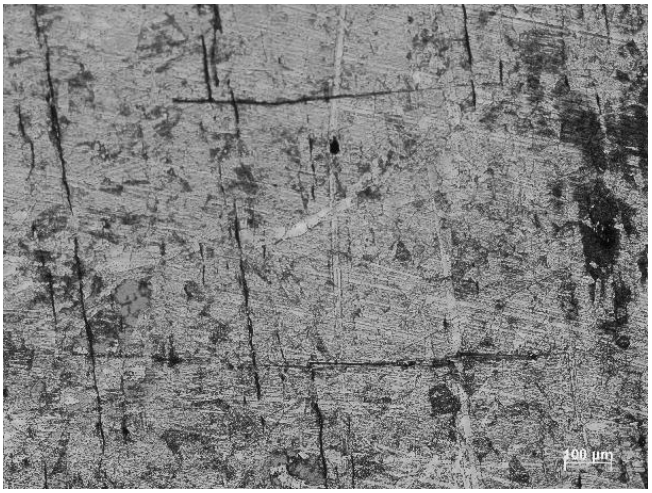

Fig. 6. Spall and shear cracks in steel (×100)

In the third target zone, associated with the interference of loading and unloading waves, two types of cracks were observed: parallel to the rear surface and shear cracks perpendicular to them (Fig. 6). The first type of cracks is caused by tensile stresses during the interference of unloading waves, and the second ones may be due to their appearance by shear stresses in a direct load wave when they reach a critical value.

Evolution of microstructure in aluminum bronze. In the first zone of the aluminum tin-free bronze target, adiabatic shear bands (ASB) were revealed as characteristic features (Fig. 7a).

In the second zone, along with ASB, there are also zones of dynamic recrystallization (Figs. 7b, 7c).

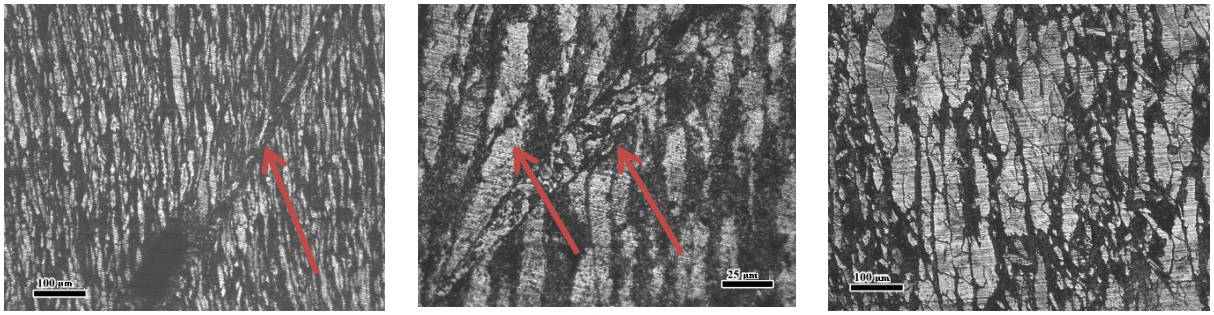

a) b) c)

Fig. 7. Adiabatic shear bands – (a, b) (indicated by arrows), dynamic recrystallization zones – (b), and recrystallized grains – (c)

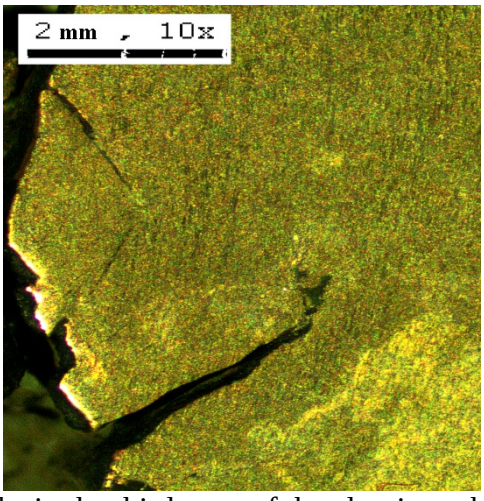

Fig. 8. Cracks in the third zone of the aluminum bronze target

In the third zone, on the sides of the cavity, there are cracks up to 3 mm long, oriented relative to the direction of the striker's action on different sides at an angle of 45º (Fig. 8).

It can be assumed that in this zone, under the conditions of the dynamic impact of the striker, compression along one axis was realized in the target, which was transformed into a volumetric oppositely deformed state, which led to the formation of the indicated oblique cracks.

Thus, based on the totality of the studies of the evolution of the microstructure of obstacle materials after a high-speed impact by a compact impactor of irregular shape, we can draw the following conclusion:

After shock loading with the penetration of targets made of different metals with an FCC lattice, signs of the transformation of the deformed state due to the dissipation of mechanical energy were revealed in the following sequence: slip of dislocations, rotational formations, and localized adiabatic shears, bands of a fragmented state and dynamic recrystallization, local dynamic polygonization and recrystallization. Structural changes are weakly dependent on the initial structure of the metal and are realized with the participation of interference (wave) effects of shock wave scattering.

4. The results of microstructural studies of specimens made of bronze of the brand BrAlFeNiMn_9-4-4-1 after tests on the Split Hopkinson Bar

Figure 9 shows the structure of the sample after loading with a strain rate of $\dot{\varepsilon}$ =915 s^{-1} when moving inward: from the fracture surface to its tail (a $\rightarrow$ d).

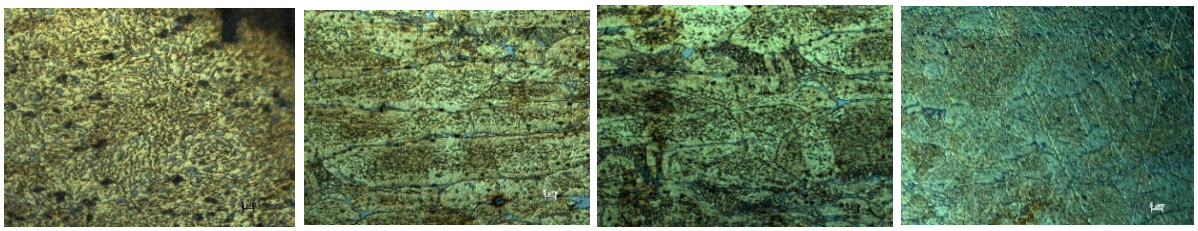

a b c d

Fig. 9. The structure of bronze brand BrAlFeNiMn_9-4-4-1 after loading SHB-1 when moving from the fracture surface deep into the sample (×1000_C_DIC)

At the fracture surface (Fig. 9a), the structure is practically grain-free - it consists of an α substitutional solution of aluminum in copper and a eutectoid $\alpha + \gamma'$ without clearly defined grain boundaries (quasi-amorphous structure). That is, it can be assumed that in this case, a certain structural phase transition occurred, which is typical for large plastic deformations [21]. When moving deeper, grains elongated along the initial rolling appear (Fig. 9b), consisting of the same two phases, the eutectoid is more often located at the grain junctions. Further, more equiaxed grains appear (Fig. 9c) with a large amount of eutectoid at their boundaries. In addition, many small cracks and pores are observed in the sample, especially near the fracture surface (Fig. 9a). In some places (Fig. 9d), twins are found, which is more typical for metals with FCC and HCP lattices, while in metals with BCC lattice they appear only at high strain rates and high pressures [22].

The characteristic structures of the sample after the rupture with a strain rate of $\dot{\varepsilon}$ = 1475 s^{-1} are shown in Fig. 10. At the discontinuity surface, the structure is similar to the structure shown in Fig. 9a. Figure 10a (slightly farther from the fracture surface) shows the region of dynamic recrystallization, and in Fig. 10b, areas of the amorphized structure are observed (residual formations from amorphization of the structure near the fracture surface). Pores and cracks are observed in the same figures. Figure 10c shows both equiaxed and elongated grains with a large amount of eutectoid.

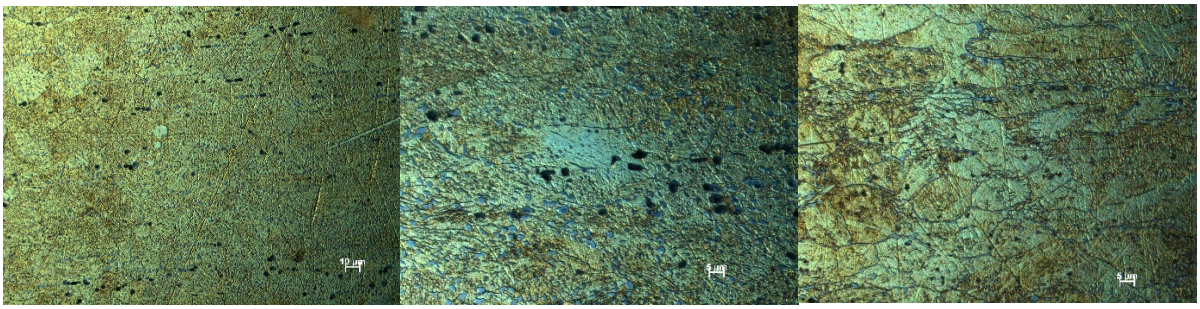

a b c

Fig. 10. Sample structure after loading with strain rate $\dot{\varepsilon}$ =1475 s^{-1}: a) ×500; b, c) ×1000 (C_DIC)

The microstructure of the sample after loading with a strain rate $\dot{\varepsilon}$ = 1750 s^{-1} in the zone slightly removed from the fracture surface (Fig. 11) differs from the microstructures of the previous samples. There are no differences near the fracture surface. Micropores and microcracks are also observed.

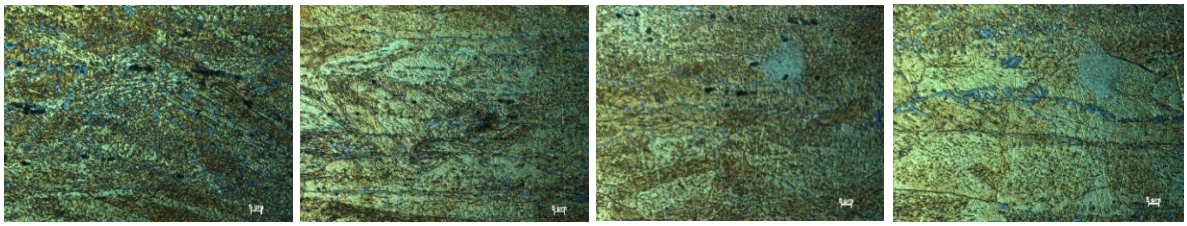

a b c d

Fig. 11. Sample structure after loading at strain rate $\dot{\varepsilon}$ =1750 s^{-1} (×1000 C_DIC)

But in Figure 11b, vortex-like structures are observed, which indicates that at higher strain rates, additional rotational modes of plastic deformation are switched on to maintain the mechanical energy dissipation rate at the required level, just as in the case of a high-speed impact with a compact impactor (see above). Figures 11c and 11d show areas of amorphization, individual twins, and localization zones.

As a result of the studies of the evolution of the structure of specimens made of bronze of the brand BrAlFeNiMn_9-4-4-1, tested at relatively low strain rates [10], it *can be stated* that it undergoes the entire spectrum of changes that is characteristic of higher values of strain rates and pressures. In addition, it was found that in the region of sample rupture, its microstructure acquires an amorphous (quasi-amorphous) form. This fact indicates that, during deformation and rupture, a structural phase transition occurred in the neck of the sample, associated with the formation of unstable excited regions. The structural-phase transition is also observed at very high strain rates [23]. In an excited state and, accordingly, during a structural-phase transition, which occurs in very short periods of time, the interaction of structures of various levels is observed, the material is in a state far from equilibrium, in which its qualitative rearrangement and an abrupt change in both the properties of the material and its aggregate state [24-26].

5. Conclusions

The study of the kinetics of the microstructure of FCC metals during high-speed penetration revealed the following mechanisms of deformation and destruction:

1. Glide of dislocations
2. Rotational deformation modes
3. Adiabatic shifts
4. Spall destruction
5. Dynamic recrystallization.

When loading at lower rates using a Hopkinson rod, the following features of the microstructure of FCC metals are locally observed, which are typical for high-speed deformation:

1. Microcracks and pores
2. Doubles
3. Dynamic recrystallization
4. Quasi-amorphous structure
5. Vortex structures

Structural changes in FCC metals under high-speed loading weakly depend on the initial structure of the metal.

References

[1] Atroshenko SA. Scale levels of dynamic translational fracture mechanisms. *Materials Physics and Mechanics*. 2016;26(1): 16-18.
[2] Mayer AE, Atroshenko SA, Borodin IN. Experimental and numerical investigations of the scale levels in spall fracture of D16 aluminum. *Materials Physics and Mechanics*. 2016;26(1): 23-25.
[3] Meshcheryakov YI, Khantuleva TA. Non-equilibrium processes in condensed media. Part 1. Experimental studies in the light of nonlocal transport theory. *Physical Mesomechanics*. 2014;17(5): 21-37.
[4] Barakhtin BK, Savenkov GG. Relationship of spall characteristics with the dimension of the fracture fractal structure. *Applied Mechanics and Technical Physics*. 2009;50(6): 61-69.
[5] Kuznetsov AV, Savenkov GG, Bragov AM, Konstantinov AY. Influence of the emerging fractal fracture surface on the dynamic properties of titanium. *Problems of Strength and Plasticity*. 2016;78(2): 218-227.
[6] Savenkov GG, Stolyarov VV, Kuznetsov AV, Meshcheryakov YI. The Nature of Fractal Relief of Fractured Metal Samples after Dynamic Loading. *Journal of Machinery Manufacture and Reliability*. 2020;49(5): 439-445.
[7] Savenkov GG, Kuznetsov AV. Dynamic Properties of Viscous Metals with a Surface Layer Modified by a Pulsed Electron Beam. In: Perspective Materials and Technologies. Vitebsk: EE "VGTU"; 2017. p.73 - 89.
[8] Orlenko LP. (Ed.) *Physics of the explosion*. Moscow: FIZMATLIT; 2002. (In Russian)
[9] Kolpakov VI, Savenkov GG, Rudomyotkin KA, Grigoriev AY. Mathematical modeling of the formation of compact projectiles from low-spherical linings. *Technical Physics*. 2016;86(8): 21-25.
[10] Bragov AM, Lomunov AK. *Using the Kolsky method to study the processes of high-speed deformation of materials of various physical nature: monograph.* Nizhny Novgorod: Publishing house of UNN; 2017. (In Russian)
[11] Morozov VA. *Dynamics of high-speed loading of materials.* St. Petersburg: Publishing House of St. Petersburg University; 2003. (In Russian)
[12] Basalin AV, Konstantinov AY, Krushka L. Development of the direct impact method for determining deformation diagrams of elastoplastic materials under large deformations. *Problems of Strength and Plasticity.* 2020;82(2): 135-146.
[13] Bragov AM, Igumnov LA, Konstantinov AY, Lomunov AK. *High-speed deformation of materials of various physical nature: monograph.* N. Novgorod; 2020.
[14] Zukas JA, Nicholas T. *Impact dynamics*. Krieger Pub Co; 1992.
[15] Merzhievsky LA, Titov VM. High-speed impact. *Physics of combustion and explosion.* 1987;23(5): 92-108.
[16] Fomin VM. (Ed.) *High-speed interaction of bodies*. Novosibirsk: Publishing house of SB RAS; 1999.
[17] Gladyshev SA, Grigoryan VA. *Armor steel*. Moscow: Intermet Engineering; 2010.
[18] Barakhtin BK, Prus AA, Savenkov GG. Microstructural features of deformation of obstacles during high-speed penetration of plane jets. *Applied Mechanics and Technical Physics*. 1989;5: 155-158.
[19] Moss JL. Influence of shock waves on the magnitude, rate and temperature of deformation in adiabatic shear bands. In: *Shock waves and phenomena of high-velocity deformation of metals*. Moscow: Metallurgy; 1984. p.30-40. (In Russian)
[20] Rybin VV. *Large plastic deformation and destruction of metals*. Moscow: Metallurgy; 1986.

[21] Pavlov VA. Amorphization of the structure of metals and alloys with an extremely high degree of plastic deformation. *Fizika Metallov i Metallovedenie*. 1985;59(4): 629-649. (In Russian)
[22] Atroshenko SA. Mechanisms of multiscale dynamic deformation and destruction of various types of metals. *Chemical Physics*. 2002;21(9): 93-99.
[23] Epstein GN, Kaibyshev OA. *High-speed deformation and structure of metals*. Moscow: Metallurgy; 1971.
[24] Murr LE. Formation of defects during deformation by a shock wave. In: Meirs MA, Murra LE. (Eds.) *Shock waves and phenomena of high-speed deformation of metals.* 1984. p.121-151. (In Russian)
[25] Epstein GN. *The structure of metals deformed by an explosion*. Moscow: Metallurgy; 1988. (In Russian)
[26] Savenkov GG, Barakhtin BK, Rudometkin KA. Investigation of structures in a copper cumulative jet using multifractal analysis. *Journal of Technical Physics*. 2015;85(1): 98-103.

THE AUTHORS

Atroshenko S.A.
e-mail: satroshe@mail.ru
ORCID: 0000-0002-5733-5915

Smakovsky M.S.
e-mail: sms84@bk.ru
ORCID: 0000-0002-2904-6200

Savenkov G.G.
e-mail: sav-georgij@yandex.ru
ORCID: 0000-0001-6069-302X